Spectral properties of the SPH Laplacian operator

Damien Violeau, Agnès Leroy, Antoine Joly, Alexis Hérault

Spectral properties of the SPH Laplacian operator

Damien Violeau (corresponding author), damien.violeau@edf.fr, Agnès Leroy, Antoine Joly, EDF R&D and Saint-Venant Laboratory for Hydraulics, Chatou, France
Alexis Hérault, Conservatoire National des Arts et Métiers, Paris, France & Istituto Nazionale di Geofisica e Vulcanologia
Catania, Italy

Abstract

In order to address the question of the SPH (Smoothed Particle Hydrodynamics) Laplacian conditioning, a spectral analysis of this discrete operator is performed. In the case of periodic Cartesian particle network, the eigenfunctions and eigenvalues of the SPH Laplacian are found on theoretical grounds. The theory agrees well with numerical eigenvalues. The effects of particle disorder and non-periodicity conditions are then investigated from numerical viewpoint. It is found that the matrix condition number is proportional to the square of the particle number per unit length, irrespective of the space dimension and kernel choice.

Keywords: SPH, Laplacian, eigenvalues, spectrum, conditioning

1. Introduction and notation

The Smoothed Particle Hydrodynamics (SPH) Lagrangian method has now reached its maturity in the field of computational mechanics. We assume the reader is familiar with SPH (see *e.g.* Monaghan, 2005; a recent review for fluid application is given *e.g.* by Violeau and Rogers, 2017). SPH being based on the motion of material particles, the differential operators are approximated with discrete operators involving sums running over the (neighbouring) particles that are within the kernel support of a given particle. Here we focus on the discrete Laplacian operator used for several purposes in SPH. For the modelling of viscous forces, several kinds of SPH Laplacian forms can be used (Violeau, 2009) and applied to the (vector) velocity field, one of the most commonly used is that of Morris *et al.* (1997). On the other, since the work of Cummins and Rudman (1999), many publications have used a similar SPH Laplacian applied to the (scalar) pressure field in order to solve a Poisson equation to deal with incompressible flows through a projection method, the so-called ISPH method

(Incompressible SPH, see Shao and Lo, 2003; Lind *et al.*, 2009, Leroy *et al.*, 2014 and 2015, among others). A similar technique is employed in other related particle-based simulation methods such as MPS (Moving Particle Semi-Implicit, see *e.g.* Koshizuka *et al.*, 1995; Khayyer and Gotoh, 2009). A review of these techniques is proposed by Ma *et al.* (2016). In this kind of work, the matrix associated to the SPH Laplacian must be inverted, and the question of its conditioning has never been addressed. Inverting this kind of matrix is also useful when applying an implicit integrator to viscous forces with low Reynolds numbers (Peer *et al.*, 2015). More generally, the spectral properties of the SPH Laplacian operators can be useful to study some numerical properties of this method, like energy modes, numerical stability (Violeau and Leroy, 2014 and 2015), or SPH convergence.

In this work we will look for the eigenfunctions and eigenvalues of the Laplacian discrete SPH operator for pressure, or rather minus the Laplacian, denoted $-\mathbf{L}$. Our final goal is to estimate the condition number of the associated matrix. We work in arbitrary dimension d (typically $d = 2$ or 3), on a Cartesian lattice of $N = n^d$ particles with distances δr and individual volumes $V = \delta r^d$, covering a square (or cubic) domain of size L^d (with $L = n\delta r$), and periodicity conditions in all directions (the case $d = 2, n = 6$ is shown in Figure 1). Hence, the N degrees of freedom are the pressures $\{p_b\}$, $b \in \{1, ..., N\}$, making an N–dimensional vector $\mathbf{P}$. The discrete Laplacian operator used in ISPH, without rigid boundaries and under the assumption of constant particle volume, reads:

$$\forall a, \left(\mathbf{LP}\right)_a = 2V \sum_b \left(p_a - p_b\right) \frac{w'_{ab}}{r_{ab}} \tag{1}$$

with usual SPH notations $r_{ab} \doteqdot |\mathbf{r}_{ab}|$, $\mathbf{r}_{ab} \doteqdot \mathbf{r}_a - \mathbf{r}_a$ and $w'_{ab} \doteqdot w'\left(r_{ab}\right)$, w being the smoothing kernel. In the following we also use the following notation:

$$W_{ab} \doteqdot -2V \frac{w'_{ab}}{r_{ab}} = W_{ba} > 0 \tag{2}$$

(the latter quantity is non-zero since the sum runs over $b \neq a$). The quantities W_{ab} are thus symmetrical; like the Laplacian they have the dimension of the inverse of a surface.

From label symmetry we know that the operator $-\mathbf{L}$ is positive:

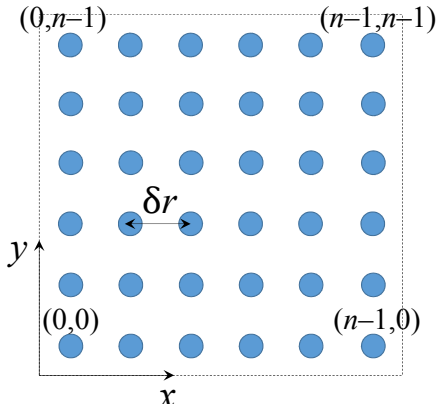

Figure 1: Cartesian periodic network of particles. Case $n = 6$, *i.e.* $N = 36$. The figures between parentheses show $(k_{1,a}, k_{2,a})$.

$$\begin{aligned} \mathbf{P}^T (-\mathbf{L}) \mathbf{P} &= \sum_{a,b} p_a (p_a - p_b) W_{ab} \\ &= \frac{1}{2} \sum_{a,b} (p_a - p_b)^2 W_{ab} \geqslant 0 \end{aligned} \tag{3}$$

This expression also shows that the kernel of $-\mathbf{L}$ (*i.e.* the set of pressure fields such that their Laplacian vanishes) is the vector line of constant pressures $\{p_b\} = \{p_0\}$.

We will first characterise multi-periodic functions on the considered particle network, then show that some of them are eigenfunctions of $-\mathbf{L}$ and identify the corresponding eigenvalues and their orders of multiplicity. The set of such eigenfunctions will be proved to make an orthonormal basis of the $-\mathbf{L}$ eigenfunctions. We will finally estimate the condition number of the $-\mathbf{L}$ matrix as a function of the domain size L and the kernel standard deviation σ.

2. Spectral analysis of the SPH Laplacian

2.1. Eigenfunctions and eigenvalues

We try to solve the following problem:

$$(-\mathbf{L}) \mathbf{P} = \lambda \mathbf{P} \tag{4}$$

which also reads

$$\forall a, \left(\lambda - \sum_b W_{ab} \right) p_a + \sum_b W_{ab} p_b = 0 \tag{5}$$

By analogy with the ordinary Laplacian and with the discrete Finite Difference Laplacian operators, we consider the vectors $\mathbf{P}$ of the form $\forall a, p_a = f_{\mathbf{K}}(\mathbf{r}_a)$, where the functions $f_{\mathbf{K}}$ are defined by

$$f_{\mathbf{K}}(\mathbf{r}) = \frac{1}{L^{d/2}} \exp(i\mathbf{K} \cdot \mathbf{r}) \tag{6}$$

$\mathbf{K} = K_j \mathbf{e}_j$ being an unknown wave vector (the normalising factor will be explained later). The spatial coordinates are defined by $\mathbf{r} = x_j \mathbf{e}_j$ ($\{\mathbf{e}_j\}$ being an orthonormal basis of $\mathbb{R}^d$) and the origin is located on the bottom left corner of the domain (in two dimensions, see Figure 1). The periodicity conditions read

$$\forall j \in \{1, ..., d\}, f_{\mathbf{K}}(\mathbf{r} + L\mathbf{e}_j) = f_{\mathbf{K}}(\mathbf{r}) \tag{7}$$

With the proposed functions, this gives

$$\forall j \in \{1, ..., d\}, e^{iLK_j} = 1 \tag{8}$$

thus

$$\forall j \in \{1, ..., d\}, K_j = \frac{2k_j\pi}{L}, k_j \in \mathbb{Z} \tag{9}$$

From now on, we denote these functions by $f_{\mathbf{k}}$, where $\mathbf{k} \doteqdot \{k_1, ..., k_d\} \in \mathbb{Z}^d$, thus $\mathbf{K} = \frac{2\pi}{L}\mathbf{k}$:

$$f_{\mathbf{k}}(\mathbf{r}) \doteqdot \frac{1}{L^{d/2}} \exp\left(\frac{2i\pi}{L}\mathbf{k} \cdot \mathbf{r}\right) \tag{10}$$

With our assumptions the particles have half-integer coordoninates, *i.e.* $x_{j,a} = \left(k_{j,a} + \frac{1}{2}\right)\delta r$, with $k_{j,a} \in \{0, ..., n-1\}$, or $\mathbf{r}_a = \left(k_{j,a} + \frac{1}{2}\right)\delta r \mathbf{e}_j$ (with a summation over the repeated label j). Then, since $L = n\delta r$:

$$\forall a, f_{\mathbf{k}}(\mathbf{r}_a) = \frac{1}{L^{d/2}} \prod_{j=1}^{d} \exp\left[\frac{2i\pi}{n} k_j \left(k_{j,a} + \frac{1}{2}\right)\right] \tag{11}$$

We now observe that these functions are redundant. Indeed we have

$$\begin{aligned} \forall j \in \{1, ..., d\}, f_{\mathbf{k}+n\mathbf{e}_j}(\mathbf{r}_a) &= f_{\mathbf{k}}(\mathbf{r}_a) \exp(2i\pi k_{j,a}) \\ &= f_{\mathbf{k}}(\mathbf{r}_a) \end{aligned} \tag{12}$$

The latter function belongs to the same vector line as $f_{\mathbf{k}}$. We thus have $N = n^d$ linearly independant periodic functions $f_{\mathbf{k}}$, given by $\mathbf{k} \in \{0, ..., n-1\}^d$. We can see that they all are eigenfunction of $-\mathbf{L}$, by dividing (5) by $f_{\mathbf{k}}(\mathbf{r}_a)$:

$$\forall a, \lambda - \sum_b W_{ab} + \sum_b W_{ab} \exp\left(-\frac{2i\pi}{L}\mathbf{k}\cdot\mathbf{r}_{ab}\right) = 0 \tag{13}$$

This relation can be satisfied by all particles a because the sums are invariant through discrete translations on the regular network. We thus have

$$\lambda_{\mathbf{k}} = \sum_b \left[1 - \exp\left(-\frac{2i\pi}{L}\mathbf{k}\cdot\mathbf{r}_{ab}\right)\right] W_{ab} \tag{14}$$

2.2. Orthogonality of the eigenbasis

The proposed eigenfunctions $f_{\mathbf{k}}$ are linearly independent since they are orthogonal with respect to the following hermitian product:

$$\langle \{f_a\}, \{g_a\} \rangle \doteqdot \delta r^d \sum_a f_a \overline{g}_a \tag{15}$$

where $\overline{z}$ denotes the complex conjugate of z. Indeed, from (11) we have

$$\begin{aligned}\langle \{f_{\mathbf{k}}(\mathbf{r}_a)\}, \{f_{\mathbf{k}'}(\mathbf{r}_a)\} \rangle &= \left(\frac{\delta r}{L}\right)^d \prod_{j=1}^{d} \sum_{k_{j,a}=0}^{n-1} \exp\left[\frac{2i\pi}{n}\left(k_j - k'_j\right)\left(k_{j,a} + \frac{1}{2}\right)\right] \\ &= \frac{1}{N}\prod_{j=1}^{d} \exp\left[\frac{i\pi}{n}\left(k_j - k'_j\right)\right] \sum_{m=0}^{n-1} \exp\left[\frac{2i\pi}{n}\left(k_j - k'_j\right)m\right] \end{aligned} \tag{16}$$

(the minus sign in front of k'_j stems from complex conjugation of $f_{\mathbf{k}'}(\mathbf{r}_a)$). We now observe that

$$Z_j \doteqdot \exp\left[\frac{2i\pi}{n}\left(k_j - k'_j\right)\right] \tag{17}$$

is an n–th complex root of 1. Hence:

$$\begin{aligned}\forall j, \sum_{m=0}^{n-1} \exp\left[\frac{2i\pi}{n}\left(k_j - k'_j\right)m\right] &= \sum_{m=0}^{n-1} Z_j^m \\ &= n\delta_{k_j k'_j}\end{aligned} \tag{18}$$

since the sum of the first n powers of Z_j vanishes unless $Z_j = 1$, *i.e.* $k_j - k'_j = 0$. Finally:

$$\langle \{f_{\mathbf{k}}(\mathbf{r}_a)\}, \{f_{\mathbf{k}'}(\mathbf{r}_a)\} \rangle = \frac{1}{N} \prod_{j=1}^{d} \exp\left[\frac{i\pi}{n}\left(k_j - k'_j\right)\right] n\delta_{k_j k'_j} \tag{19}$$
$$= \delta_{\mathbf{k}\mathbf{k}'}$$

3. Analysis of the spectrum

3.1. Counting the eigenvalues

We saw that the eigenvalues are given by (14), which also reads

$$\lambda_{\mathbf{k}} = \sum_b \left[1 - \cos\left(\frac{2\pi}{L}\mathbf{k}\cdot\mathbf{r}_{ab}\right)\right] W_{ab} \geqslant 0 \tag{20}$$
$$\mathbf{k} \in \{0, ..., n-1\}^d$$

This is because the contribution of the sinus terms cancels out by symmetry, since for all particle b there is another one b' such that $\mathbf{r}_{ab'} = -\mathbf{r}_{ab}$, with $W_{ab'} = W_{ab}$:

$$\sum_b \sin\left(\frac{2\pi}{L}\mathbf{k}\cdot\mathbf{r}_{ab}\right) W_{ab} = 0 \tag{21}$$

The fact that the eigenvalues (20) are real and positive is natural since the matrix of $-\mathbf{L}$ is symmetrical and positive. As we said in the introduction, it is positive definite only for non constant pressure fields. We must now remove the constant pressure fields, given by the vector line of eigenfunctions directed by $f_{\mathbf{0}}$ (this is possible since the pressure is only defined up to an additive constant value). We must thus remove the set $\mathbf{k} = (0, ..., 0)$, which amounts to removing the eigenvalue $\lambda_{\mathbf{0}} = 0$. This can be done by imposing the pressure of one particle, reducing the number of degrees of freedom (or eigenmodes) to $N - 1$.

It is obvious that several eigenfunctions can correspond to the same eigenvalue. Indeed, using the notation $k_{j,ab} \doteqdot k_{j,a} - k_{j,b}$ we have

$$\forall j \in \{1, ..., d\}, \lambda_{n\mathbf{e}_j - \mathbf{k}} = \sum_b \left[1 - \cos\left(2\pi k_{j,ab} - \frac{2\pi}{L}\mathbf{k}\cdot\mathbf{r}_{ab}\right)\right] W_{ab} \tag{22}$$
$$= \sum_b \left[1 - \cos\left(\frac{2\pi}{L}\mathbf{k}\cdot\mathbf{r}_{ab}\right)\right] W_{ab}$$
$$= \lambda_{\mathbf{k}}$$

Thus, every coordinate k_j of $\mathbf{k}$ leads to the same eigenvalue as $k'_j = n - k_j$. The values of k_j can thus be paired, except 0 and $\frac{n}{2}$ (if n is even). This holds in all spatial

directions, which leaves only $\left(\left\lfloor \frac{n}{2} \right\rfloor + 1\right)^d - 1$ distinct non-zero eigenvalues. This is still reduced by noting that the k_j can be swapped by space isotropy. Thus, we can write the k_j by decreasing order: there are $\left\lfloor \frac{n}{2} \right\rfloor + 1$ choices for k_1 $(0, ..., \left\lfloor \frac{n}{2} \right\rfloor)$, then $k_1 + 1$ choices for k_2 $(0, ..., k_1)$, etc. Finally, there are

$$\binom{\left\lfloor \frac{n}{2} \right\rfloor + 2}{d} - 1 \tag{23}$$

distinct non-zero eigenvalues, unless other distincts sets of integers give the same result using (20). This reasonning also shows that when n is large, most of the eigenvalues have the order of multiplicity 2^d.

3.2. Approximation of the eigenvalues

When the number of particles is large, the formula (20) can be approximated by an integral:

$$\lambda_{\mathbf{k}} \approx 2 \int_{\mathbb{R}^d} \left[\cos\left(\mathbf{K} \cdot \mathbf{r}\right) - 1\right] \frac{w'\left(r\right)}{r} d\mathbf{r} \tag{24}$$

This integral can be extended to the whole space if a is placed at the center of the domain and chosen as the origin in (24), the support of the kernel being smaller than $L/2$. It is related to the dimensionless function F_2 defined by Violeau & Leroy (2014, 2015):

$$F_2\left(K^*\right) = 2\sigma^2 \int_{\mathbb{R}^d} \left[\cos\left(\mathbf{K} \cdot \mathbf{r}\right) - 1\right] \frac{w'\left(r\right)}{r} d\mathbf{r} \tag{25}$$

with $K^* \doteq \sigma K$ and $K \doteq |\mathbf{K}|$. As a reminder, the kernel standard deviation is defined by

$$\sigma^2 \doteq \frac{1}{d} \int_{\mathbb{R}^d} r^2 w\left(r\right) d\mathbf{r} \tag{26}$$

Hence:

$$\lambda_{\mathbf{k}} \approx \frac{1}{\sigma^2} F_2\left(K^*\right) \tag{27}$$

It is interesting to note that this approximation does not break the positivity of eigenvalues, since F_2 is positive regardless of the kernel choice (since $w'\left(r\right) \leqslant 0$). We also notice that the eigenvalues have the dimension of the inverse of a surface, as expected. Finally, we note that with the present approximation $\lambda_{\mathbf{k}}$ only depends on the norm of $\mathbf{K}$. As a consequence, for a given choice of $\mathbf{k}$ there may be other vectors

$\mathbf{k}'$ giving the same approximation (27) of $\lambda_{\mathbf{k}}$. As a consequence, the approximation (27) can fail in predicting the orders of multiplicity of the eigenvalues (examples will be provided later).

The norm of the wave vector is

$$K = \frac{2\pi}{L}\sqrt{\sum_{j=1}^{d} k_j^2} \tag{28}$$

thus

$$\lambda_{\mathbf{k}} \approx \frac{1}{\sigma^2} F_2\left(2\pi \frac{\sqrt{\sum_{j=1}^{d} k_j^2}}{n} \frac{\sigma}{\delta r}\right) \tag{29}$$

3.3. Condition number of the SPH Laplacian

The condition number of positive definite matrix is given by the ratio of its extreme eigenvalues. With (29) we obtain, for large n:

$$\lambda_{\min} = \lambda_{(1,\dots,0)^T} \approx \frac{1}{\sigma^2} F_2\left(\frac{2\pi}{n}\frac{\sigma}{\delta r}\right) \tag{30}$$

$$\lambda_{\max} = \lambda_{\left(\lfloor \frac{n}{2} \rfloor,\dots,\lfloor \frac{n}{2} \rfloor\right)^T} \approx \frac{1}{\sigma^2} F_2\left(\pi\sqrt{d}\frac{\sigma}{\delta r}\right) \tag{31}$$

We note that $\lambda_{\min}$ depends on $\frac{\sigma}{L}$, while $\lambda_{\max}$ depends on $\frac{\sigma}{\delta r}$. Thus both discretization parameters have an effect, each of them at one side of the spectrum.

To go further in estimating the condition number, we use Violeau et Leroy's results (2014):

$$F_2\left(K^*\right) \underset{K^* \longrightarrow 0}{\sim} K^{*2} \tag{32}$$

$$F_2\left(K^*\right) \underset{K^* \longrightarrow +\infty}{\longrightarrow} F_\infty \tag{33}$$

F_2 is plotted in Figure 2 for the Gaussian kernel on one hand, and for Wendland's 5th order kernel in dimension 2 on the other hand (Wendland, 1995). The asymptotic value F_∞ given in (33) is equal to 2 for the Gaussian kernel irrespective of d, and remains close to 2 for other types of kernels (this asymptote is reached when $K^* \approx 4$). Now, for usual SPH simulations $\pi\sqrt{d}\frac{\sigma}{\delta r} \sim 10$, showing that increasing $\frac{\sigma}{\delta r}$ has almost no effect on $\lambda_{\max}$. Moreover, the factor $\frac{1}{n}$ in $\lambda_{\min}$ (equation (30)) allows using the approximation of F_2 for small values of K^* (equation (32)). Hence:

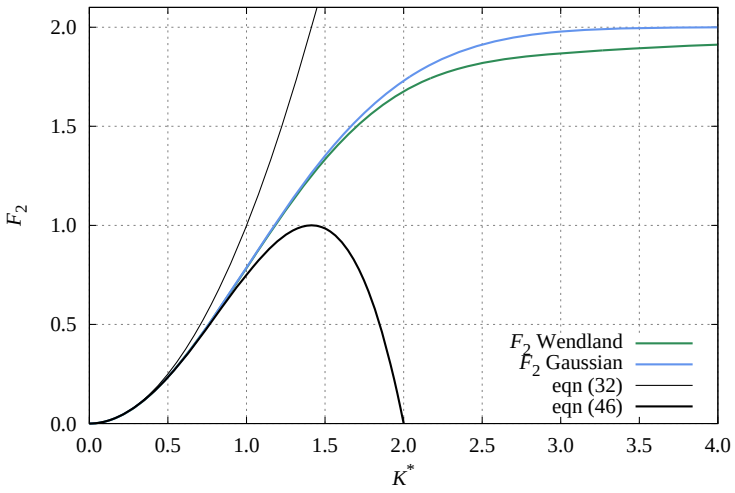

Figure 2: Graph of $F_2\,(K^*)$ for the Gaussian kernel and Wendland's 5th order kernel in dimension $d = 2$. The black lines represent the approximations near the origin (32) (thin line) and (46) (thick line), respectively.

$$\lambda_{\min} \approx \left(\frac{2\pi}{L}\right)^2 \tag{34}$$

$$\lambda_{\max} \approx \frac{F_\infty}{\sigma^2} \tag{35}$$

The condition number of $-\mathbf{L}$ is thus given, as an approximation, by

$$\begin{aligned}\frac{\lambda_{\max}}{\lambda_{\min}} &\approx F_\infty \left(\frac{1}{2\pi}\frac{L}{\sigma}\right)^2 \\ &= F_\infty \left(\frac{n}{2\pi}\frac{\delta r}{\sigma}\right)^2\end{aligned} \tag{36}$$

This is a very bad conditioning, similar to that of Finite Differences (Allaire & Kaber, 2008). It is an increasing function of n, meaning that refining the discretisation can increase the numerical error. One can observe that it is proportional to n^2 regardless of the space dimension. Besides, it is independent on the number of particles within the kernel support in the present approximation, which is a consequence of the fact that $\lambda_{\max}$ is almost independent on $\frac{\sigma}{\delta r}$). Finally, one can notice that

making the particle coordinates dimensionless would not improve the conditioning, since the ration $\frac{L}{\sigma}$ would remain unchanged.

3.4. Case of the continuous SPH Laplacian

In the case of a large number of particles within the kernel support, the discrete sums can be approximated by integrals, showing that the eigenfunctions and eigenvalues are almost independent on the particle distribution. We can solve the following eigenvalue problem similarly to what has been done so far:

$$\forall \mathbf{r}, \int_{[0,L]^d} \left[p\left(\mathbf{r}\right) - p\left(\mathbf{r}'\right)\right] W\left(\left|\mathbf{r} - \mathbf{r}'\right|\right) d\mathbf{r}' = \lambda p\left(\mathbf{r}\right) \tag{37}$$

where W is defined as above: $W\left(r\right) = -2w'\left(r\right)/r$. We seek for orthogonal eigenfunctions in the form given by (6). The periodicity condition imposes that the wave vector satisfies the same conditions as in the discrete case (9), but without restrictions to $\mathbf{k}$, which can now be chosen arbitrarily in $\mathbb{Z}^d$. A development similar to (13) gives, using the variable change $\tilde{\mathbf{r}} \doteqdot \mathbf{r}' - \mathbf{r}$:

$$\begin{aligned} \lambda_{\mathbf{k}} &= \int_{[0,L]^d} \left[1 - \exp\left(-i\mathbf{K}\cdot\tilde{\mathbf{r}}\right)\right] W\left(\tilde{r}\right) d\tilde{\mathbf{r}} \\ &= 2\int_{[0,L]^d} \left[\cos\left(\mathbf{K}\cdot\tilde{\mathbf{r}}\right) - 1\right] \frac{w'\left(\tilde{r}\right)}{\tilde{r}} d\tilde{\mathbf{r}} \\ &= \frac{1}{\sigma^2} F_2\left(K^*\right) \end{aligned} \tag{38}$$

(if $L/2$ is larger than the kernel support). We thus get an infinity of eigenvalues, given by the same formula as in the discrete case, but this time without any approximation. This spectrum represents the limit of the discrete Cartesian case when $\delta r/\sigma$ is very small. This result shows that the particle arrangement has only little effect on the condition number when using many particles in the kernel support.

The eigenfunctions (6) are orthonormal with respect to the following hermitian product:

$$\left(f, g\right) \doteqdot \int_{[0,L]^d} f\left(\mathbf{r}\right) \overline{g}\left(\mathbf{r}\right) d\mathbf{r} \tag{39}$$

Indeed, we have:

$$\begin{aligned} \left(f_{\mathbf{K}}, f_{\mathbf{K}'}\right) &= \frac{1}{L^d} \int_{[0,L]^d} \exp\left[\frac{2i\pi}{L}\left(\mathbf{k} - \mathbf{k}'\right)\cdot\mathbf{r}\right] d\mathbf{r} \\ &= \delta_{\mathbf{k}\mathbf{k}'} \end{aligned} \tag{40}$$

On the other hand, on decreasing σ (yet in the continuous case) the norms of the wave vectors K^* are decreased. According to (32), the eigenvalues (38) thus behave as follows:

$$\lambda \sim K^2 \tag{41}$$

These are the eigenvalues of the $-\Delta$ operator, as expected. Hence, the spectrum of the SPH Laplacian operator tends towards the spectrum of the true Laplacian operator when δr and σ are decreased while $\sigma/\delta r$ is increased. This gives a promising clue to study the convergence of the ISPH Poisson equation.

4. Examples

4.1. Cartesian case

We first concentrate on the Cartesian case with $n = 10$; we thus have $\lfloor \frac{n}{2} \rfloor = 5$. Wendland's 5th order kernel is chosen, given by

$$w(q) = \frac{7}{4\pi h^2} \left(1 - \frac{q}{2}\right)_+^4 (1 + 2q) \tag{42}$$

where $q \doteqdot r/h$, the subscript + denoting the positive value. In dimension $d = 2$, for this kernel $\sigma = \sqrt{\frac{5}{18}} h$ and $F_\infty = \frac{35}{18}$, while

$$h^2 W(q) = \frac{35}{2\pi h^2} \left(\frac{\delta r}{h}\right)^2 \left(1 - \frac{q}{2}\right)_+^3 \tag{43}$$

and

$$F_2(K^*) = \frac{35}{18} - \frac{175}{6K^{+4}} \left[\begin{array}{c} K^{+2} J_0(2K^+) - \frac{1}{2} K^+ J_1(2K^+) \\ + \frac{\pi}{2} \left(K^{+2} - \frac{3}{4}\right) Y(2K^+) \end{array} \right] \tag{44}$$

with $K^+ \doteqdot (h/\sigma) K^* = hK$ and

$$Y(x) \doteqdot J_1(x) H_0(x) - J_0(x) H_1(x) \tag{45}$$

(Violeau and Leroy, 2014). In the latter equation, J_0 and J_1 are Bessel functions of the first kind while H_0 et H_1 are the so-called Struve functions (see Abramovic & Stegun, 1972).

We consider three values of $h/\delta r = 1.5$, 2.0 and 2.5, *i.e.* $\sigma/\delta r = 0.79057$, 1.05409 and 1.31762. The norms of the wave vectors are given by (28) with $L = 10\delta r$. We

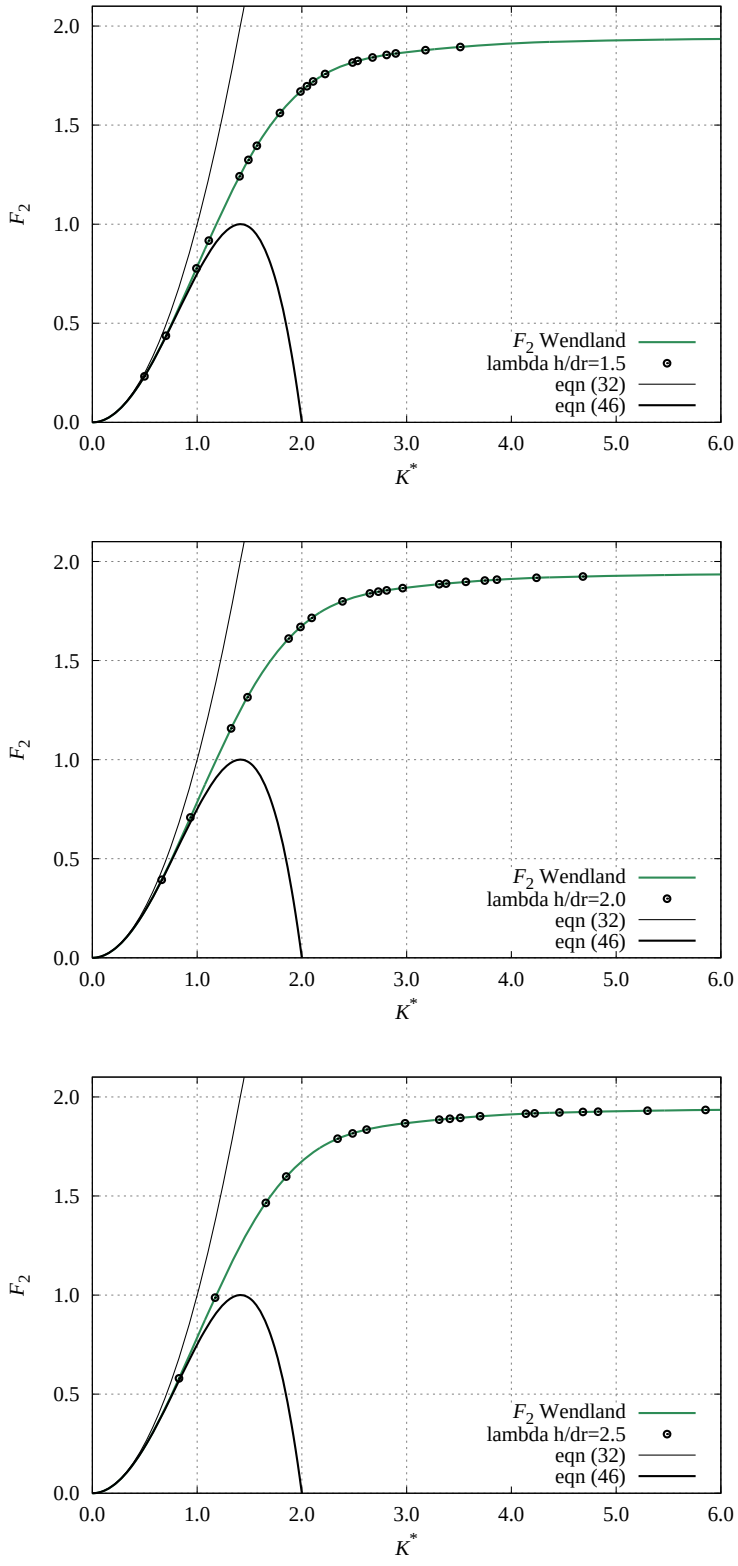

Figure 3: Graph of $F_2\,(K^*)$ for Wendland's 5th order kernel in dimension $d = 2$. The circles show the dimensionless eigenvalues $\sigma^2\lambda_{\mathbf{k}}$ as a function of the wave vector norm, in the discrete periodic Cartesian case with $n = 10$ for $h/\delta r = 1.5$, 2.0 and 2.5 (from top to bottom). The black lines represent the approximations near the origin (32) (thin line) et (46) (thick line), respectively.

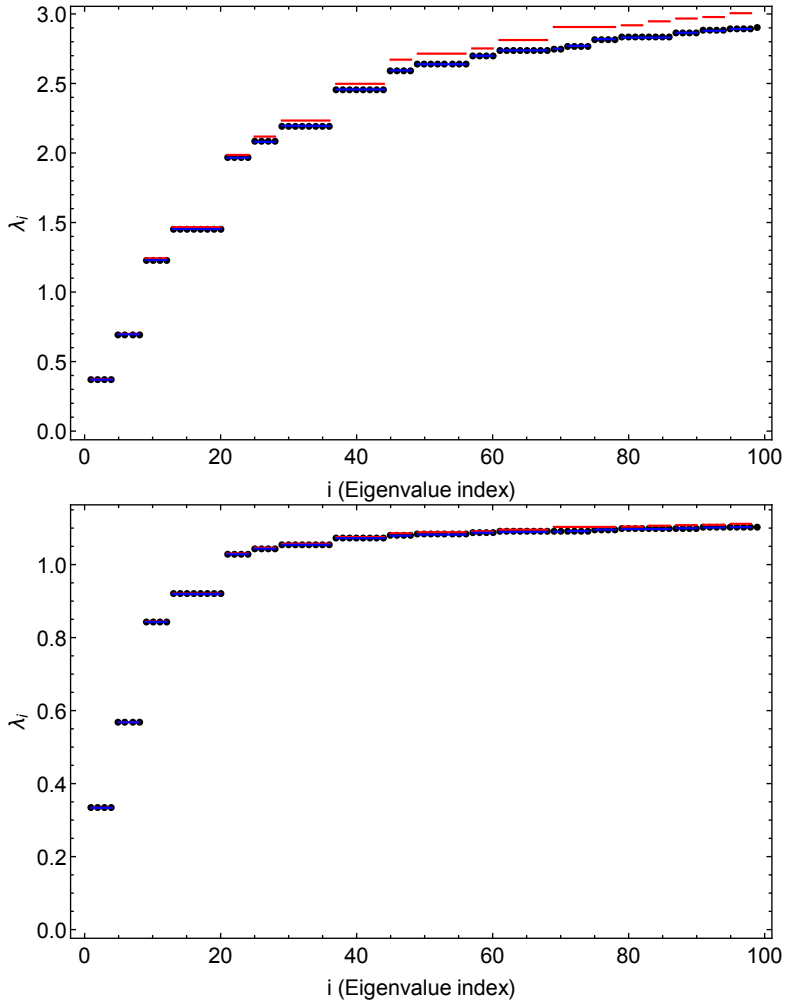

Figure 4: Discrete periodic Cartesian case with $d = 2$ and $n = 10$, Wendland's 5th order kernel. Distribution of the 19 distinct eigenvalues for $h/\delta r = 1.5$ (top) and 2.5 (bottom), using Mathematica (circles), exact theoretical values (equation (20), blue symbols) and approximate theoretical values (equation (29), red symbols). The length of horizontal bars show the orders of multiplicity.

denote here $\mathbf{k} = (k, \ell)$ (instead of (k_1, k_2)). According to (23), there are $\binom{7}{2} - 1 = 20$ distinct non-zero eigenvalues. However, we observe that the pair $(k, \ell) = (0, 5)$ yields the same value of $k^2 + \ell^2$ than $(3, 4)$ (in addition to $(5, 0)$ and $(4, 3)$). Therefore, in the approximation (29) these pairs correspond to a unique eigenvalue with order of multiplicity larger than 8 (*i.e.* 10 in the present case).

The approximate eigenvalues (29) are listed in Table 1 in the case $h/\delta r = 2.0$, by increasing order and non-dimensionalised by $1/\delta r^2$. Their orders of multiplicity $N_{\mathbf{k}}$ are also displayed, with total sum equal to $100 - 1 = 99$ as expected. They are also plotted on Figure 3, non-dimensionalised by $1/\sigma^2$.

The exact eigenvalues, given by (20), are *a priori* slightly different. This is confirmed by Figure 4, plotting the exact eigenvalues (20) as well as approximate ones (29), for two values of $h/\delta r$. the same figure also shows the numerical eigenvalues computed using Mathematica, which coincide with the present theory (20), including the orders of multiplicity. One can see that the approximate formula overestimates $\lambda_{\mathbf{k}}$. It is better when more particles are included in the kernel support (large $h/\delta r$), as expected. Figure 4 also confirms that with this approximation some orders of multiplicity are not well predicted.

The condition numbers for the three cases are given in Table 2. One can see that the formula (36) is only a crude approximation. This is because the extreme eigenvalues are only roughly estimated by (34) and (35) in this case, as evidenced by Figure 3. This is due to the small number of particles. In order to improve this estimation, one can refine (32) by

$$F_2\left(K^*\right) \underset{K^* \longrightarrow 0}{\sim} K^{*2} - \frac{K^{*4}}{4} \tag{46}$$

(Violeau & Leroy, 2014). Hence, (34) and (36) become

$$\lambda_{\min} \approx \left(\frac{2\pi}{L}\right)^2 \left[1 - \left(\frac{\pi\sigma}{L}\right)^2\right] \tag{47}$$

$$\frac{\lambda_{\max}}{\lambda_{\min}} \approx \frac{F_\infty\left(\frac{1}{2\pi}\frac{L}{\sigma}\right)^2}{1 - \left(\pi\frac{\sigma}{L}\right)^2} \tag{48}$$

Table 2 shows that this improves the prediction of condition numbers. However, the best is to invoke the accurate formulae (30) and (31). The approximations (36) and (48) are useful to study the behaviour of the conditioning with the problem parameters.

Table 1: Discrete Cartesian case with $d = 2$ and $n = 10$, Wendland's 5th order kernel. Values of the 19 norms of the dimensionless wave vectors K^+ and associated dimensionless eigenvalues $\lambda_{\mathbf{k}}$ approximated by (29), with their orders of multiplicity $N_{\mathbf{k}}$. The pairs $(3, 4)$ and $(0, 5)$ correspond to the same eigenvalue in this approximation, thus the first of these pairs does not appear explicitely.

$\mathbf{k} = (k, \ell)$	$N_{\mathbf{k}}$	K^+	$\delta r^2 \lambda_{\mathbf{k}}$
$(0, 1)$	4	1.2566	0.3543
$(1, 1)$	4	1.7772	0.6376
$(0, 2)$	4	2.5133	1.0423
$(1, 2)$	8	2.8099	1.1837
$(2, 2)$	4	3.5543	1.4498
$(0, 3)$	4	3.7699	1.5026
$(1, 3)$	8	3.9738	1.5436
$(2, 3)$	8	4.5309	1.6190
$(0, 4)$	4	5.0266	1.6551
$(1, 4)$	8	5.1813	1.6627
$(3, 3)$	4	5.3315	1.6690
$(2, 4)$	8	5.6199	1.6790
$(0, 5)$	10	6.2832	1.6966
$(1, 5)$	4	6.4076	1.6994
$(2, 5)$	4	6.7672	1.7070
$(4, 4)$	4	7.1086	1.7134
$(3, 5)$	4	7.3274	1.7170
$(4, 5)$	4	8.0464	1.7257
$(5, 5)$	1	8.8858	1.7315

On the other hand, the simple formula (36) should work better for larger values of n, the spectrum being much larger (recall that the number of degrees of freedom is $n^d - 1$). As an illustration, Figure 5 shows the wave numbers in the case $n = 40$ with $h/\delta r = 2.0$. There are now 197 distinct non-zero eigenvalues in the approximation (27), with many pairs (k, ℓ) giving identical values, *e.g.* $(0, 5) \sim (3, 4)$ (as before), $(1, 7) \sim (5, 5)$, $(1, 8) \sim (4, 7)$, $(2, 9) \sim (6, 7)$, $(1, 18) \sim (6, 17) \sim (10, 15)$, etc. The condition number is thus equal to 70.06 according to (30) and (31), while the approximations (36) and (48) give 70.92 and 71.41, respectively. Figure 6 shows the distribution of eigenvalues in this case (actually for $n = 39$), with comparison of theory against numerical values. Again we see that the exact theoretical predictions are in perfect agreement with the numerical eigenvalues, while the approximate the-

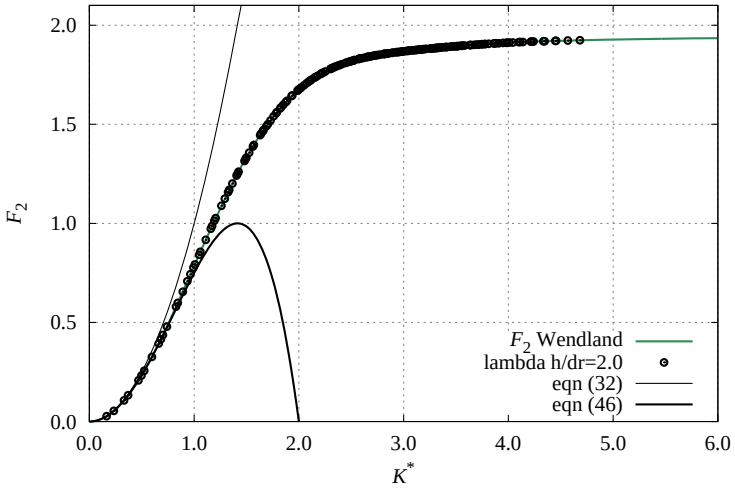

Figure 5: Graph of $F_2\,(K^*)$ for Wendland's 5th order kernel in dimension $d = 2$. The circles show the dimensionless eigenvalues $\sigma^2\lambda_{\mathbf{k}}$ as a function of the wave vector norm, in the discrete periodic Cartesian case with $n = 40$ for $h/\delta 2.0$. The black lines represent the approximations near the origin (32) (thin line) and (46) (thick line), respectively.

oretical eigenvalues using the F_2 function are overestimated. The overestimation is worst for larger eigenvalues since they correspond to smaller wave lengths.

Table 2: Discrete Cartesian case with $d = 2$ and $n = 10$, Wendland's 5th order kernel. Condition numbers of the Laplacian for the three chosen values of $\frac{h}{\delta r}$.

$\frac{h}{\delta r}$	1.5	2.0	2.5
eqns (30) and (31)	8.1626	4.8877	3.3379
eqn (36)	7.8805	4.4328	2.8370
eqn (48)	8.3986	4.9788	3.4236

4.2. Non-Cartesian cases

In order to look at the effect of particle disorder, we used Mathematica to compute the discrete Laplacian eigenvalues for a set of 39×39 particles initially placed on a Cartesian grid and then moved according to the ISPH equations in a lid-driven square cavity (hereafter referred to as LDC, we used the model by Leroy *et al.*, 2014). The distribution of the particles is shown in Figure 7, while Figure 8 shows the eigenvalues

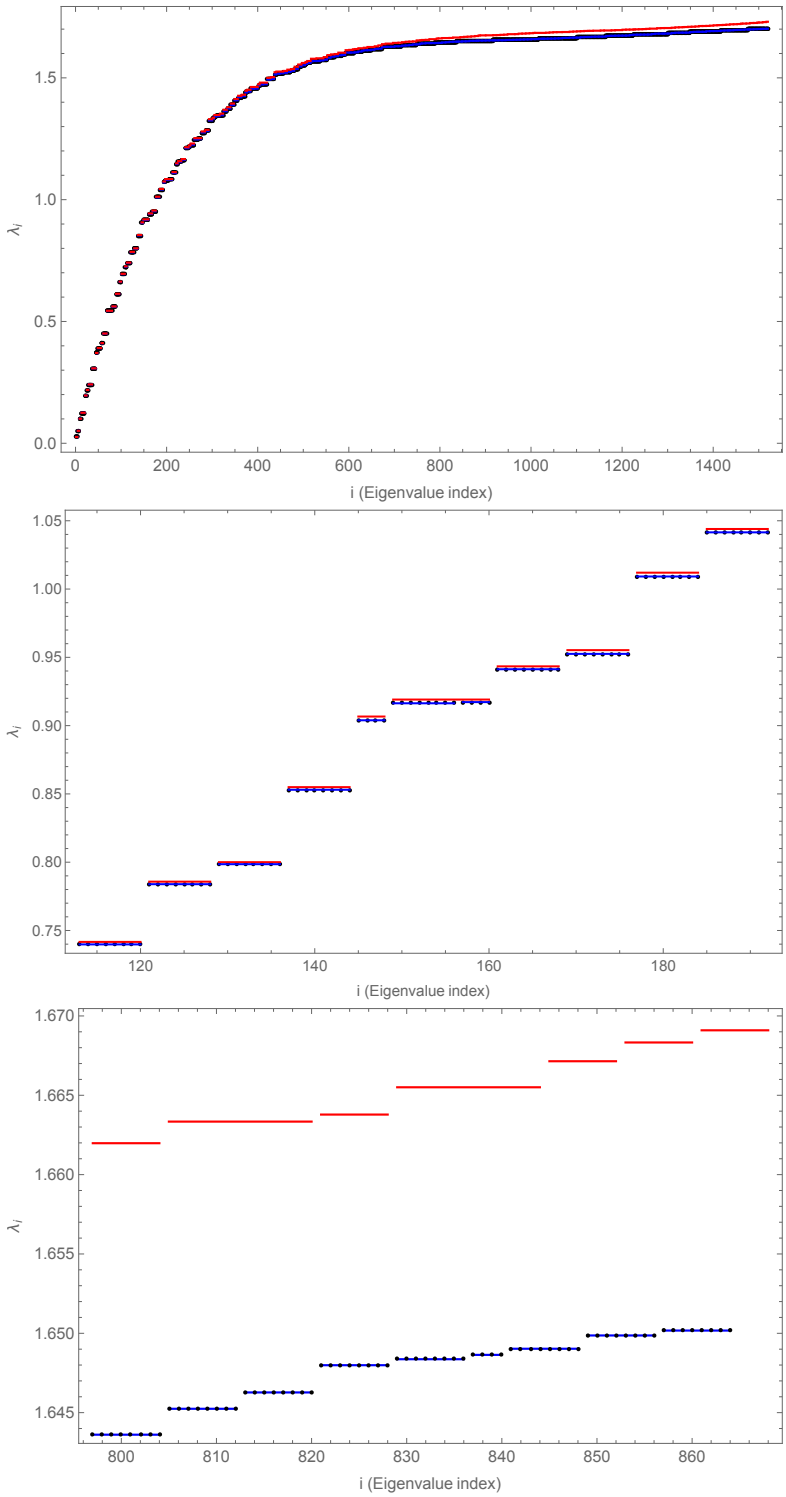

Figure 6: Discrete periodic Cartesian case with $d = 2$ and $n = 39$, Wendland's 5th order kernel. Distribution of the eigenvalues for $h/\delta r = 2.0$, using Mathematica (circles), exact theoretical values (equation (20), blue symbols) and approximate theoretical values (equation (29), red symbols). The length of horizontal bars show the orders of multiplicity. The top picture shows all eigenvalues while zooms are displayed below.

compared to the Cartesian case with the same number of particles (note that the walls of the cavity were removed, thus the domain size has been decreased by half the initial particle spacing to keep the particle density homogeneous near the periodicity boundaries). It can be seen that particle disorder has no effect on the spectrum except a small peak on the highest values, thus the condition number is almost unchanged. The reason for the increase of highest eigenvalues seems difficult to explain. They correspond to wavelenghts of typically one particle spacing, suggesting that this behaviour may be due to the local properties of the particle distribution. A careful study of these properties in SPH, such as the correlation spectrum of particle distances, remains to be done, although recent works suggest that the particle distribution in practical SPH simulation may revele non-obvious properties. As an example, Colagrossi *et al.* (2012) show that the equilibrium particle distributions in two dimensions are not obtained on regular packings. As a second non-Cartesian test case, we consider a particle distribution based on the 2-D Taylor-Green vortices (TGV) with 101×101 particles. Figure 9 shows that for the TGV case the spectrum is very similar to the Cartesian case, except that the asymptotic value is slightly reduced.

4.3. Effects of non-periodicity

The effect of periodicity is now numerically investigated. The 39×39 case with $h/\delta r = 2.0$ is considered with Mathematica with and without periodicity conditions, on Cartesian and non-Cartesian particle distributions. Figure 10 shows that with non-periodicity (*i.e.* when the particles on the boundary are considered like free-surface particles), the eigenvalues in the Cartesian case are distributed on a continuous curve with two steps (in the present case). On the other hand, the eigenvalues remain smoothly distributed when using a non-Cartesian particle distribution, while the peak on highest values is smaller than in the periodic case. On the other hand, Figure 11 shows that non-periodicity affects the intermediate eigenvalues that are smaller than in the periodic case. However, in all cases the extreme eigenvalues are almost unaffected, except the small peak on highest values. The fact that intermediate eigenvalues are decreased by non-periodicity is not clear. They correspond to wavelengths of a few particle spacings (typically the size of the kernel support, suggesting that the particle near the 'free surfaces' are responsible for this behaviour.

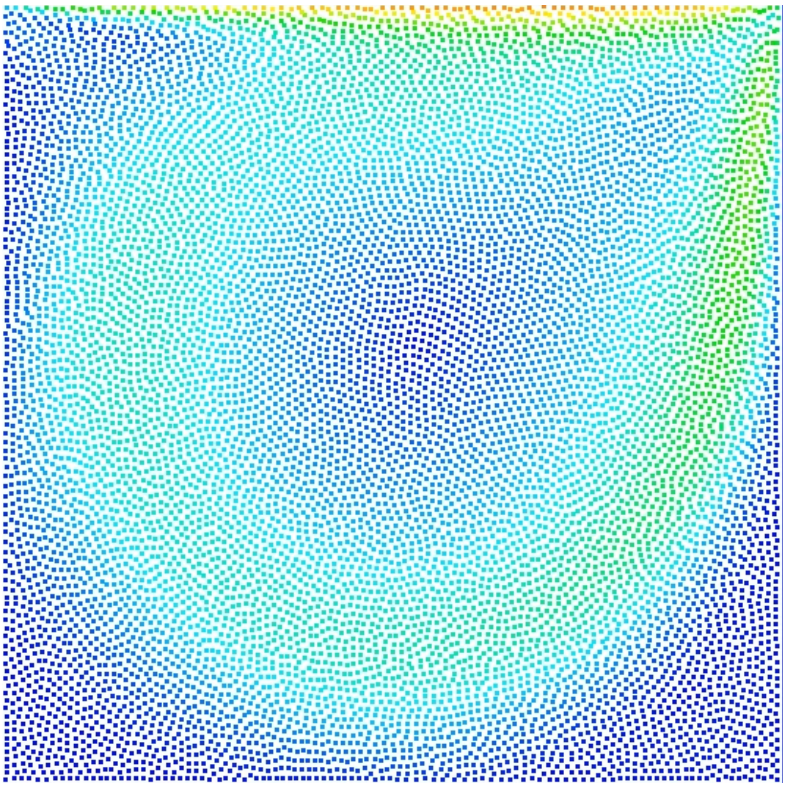

Figure 7: Discrete periodic case with $d = 2$ and $n = 39$. Distribution of particles for the first non-Cartesian (from the LDC ISPH simulation).

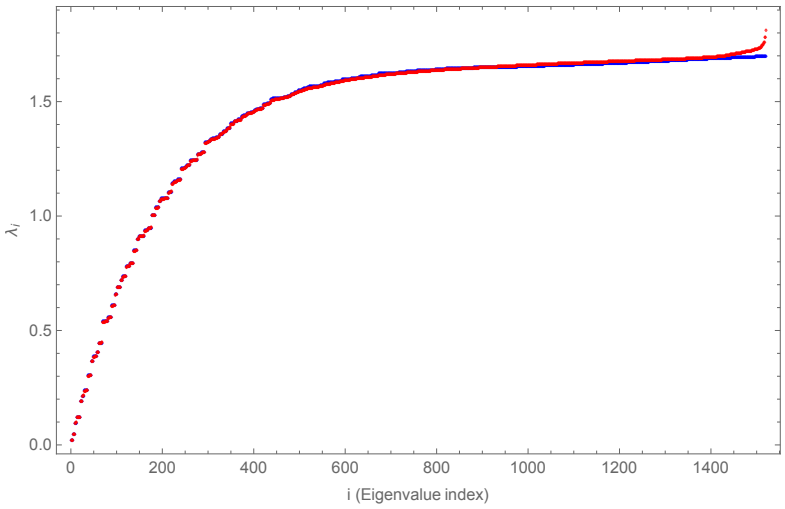

Figure 8: Discrete periodic case with $d = 2$ and $n = 39$, Wendland's 5th order kernel. Distribution of eigenvalues for $h/\delta r = 2.0$ using Mathematica. Cartesian (blue symbols) *vs.* non-Cartesian from the LDC case (red symbols).

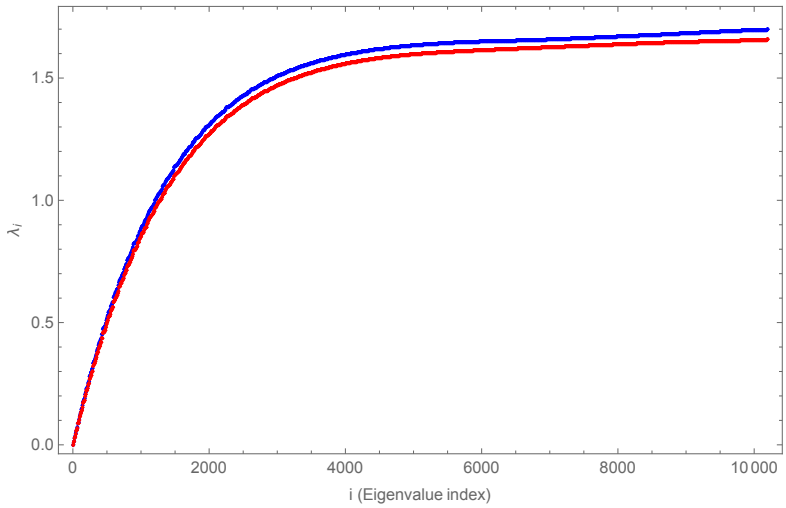

Figure 9: Discrete periodic case with $d = 2$ and $n = 101$, Wendland's 5th order kernel. Distribution of eigenvalues for $h/\delta r = 2.0$ using Mathematica. Cartesian (blue symbols) *vs.* non-Cartesian from the TGV case (red symbols).

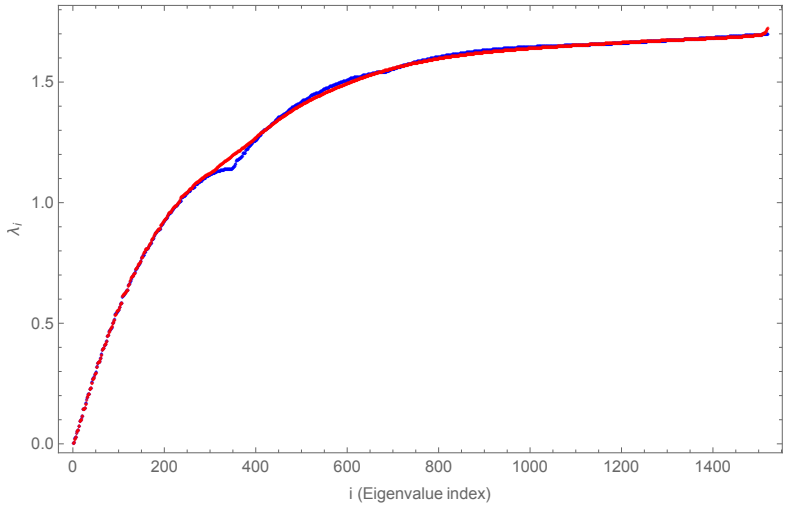

Figure 10: Discrete non-periodic case with $d = 2$ and $n = 39$, Wendland's 5th order kernel. Distribution of eigenvalues for $h/\delta r = 2.0$ using Mathematica. Cartesian (blue symbols) *vs.* non-Cartesian from the LDC case (red symbols).

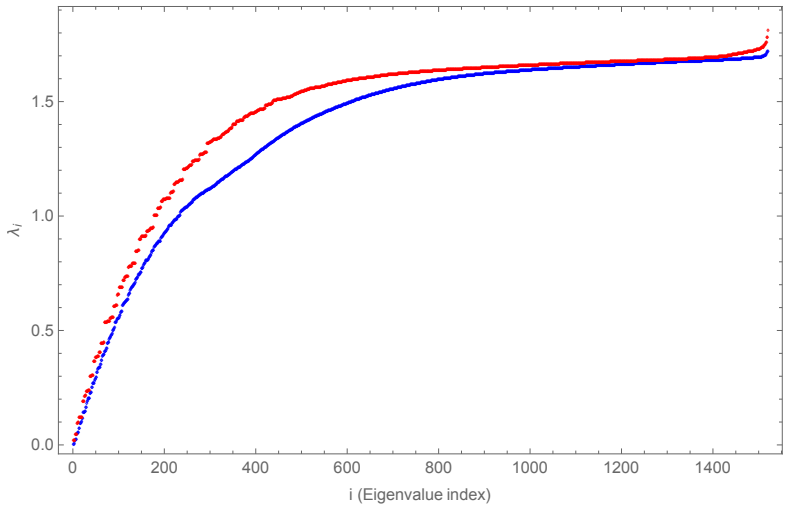

Figure 11: Discrete non-Cartesian case from the LDC with $d = 2$ and $n = 39$, Wendland's 5th order kernel. Distribution of eigenvalues for $h/\delta r = 2.0$ using Mathematica. Periodic (red symbols) *vs.* non-periodic conditions (blue symbols).

5. Conclusion

The present spectral analysis of the SPH Laplacian operator shows that its conditioning is high, being proportional to the square of the number of particles per unit length, as in Finite Differences. The exact theoretical eigenvalues agree well with numerical values in the case of a Cartesian periodic network of particles, and numerical values show that particle disorder has little effect on the condition number, while non-periodicity (*i.e.* free surface boundaries) only decrease the intermediate eigenvalues, leaving the Laplacian conditioning almost unchanged. We should emphasize that the present study being done on a square domain under steady conditions, the effect of free surface and particle disorder in ISPH may be more important with more realistic geometries and moving free surface, as suggested by practioners. A more complete study involving realistic flows remains to be done. The effect of walls also still remains to be addressed. This is a challenging work that depends on the way walls are modeled in ISPH (see Leroy *et al.*, 2014 for a consistent method). It is hard to guess wether walls will modify the conditioning of the discrete Poisson equation in a significant way.

The present theory can be useful to propose conditioning strategies, and gives clues for studying the convergence properties of the discrete ISPH Poisson equation. This could be done by decomposing the solution to the continuous and discrete Poisson

equations on their respective bases of eigenfunctions (see Violeau *et al.* for a first attempt).

References

[1] M. Abramowitz, I.A. Stegun, *Handbook of Mathematical Functions with Formulas, Graphs, and Mathematical Tables*, Dover Publications, New York, 1972 (10^{th} edition).

[2] G. Allaire, S.M. Kaber, *Numerical Linear Algebra*, Springer, New York, 2008.

[3] S.J. Cummins, M.J. Rudman (1999), *An SPH Projection Method*, J. Comput. Phys., **152**:584607.

[4] A. Colagrossi, B. Bouscasse, M. Antuono, S. Marrone (2012), *Particle packing algorithm for SPH schemes*, Comput. Phys. Comm., **183**:16411653.

[5] A. Khayyer, H. Gotoh (2009), *Modified moving particle semi-implicit methods for the prediction of 2D wave impact pressure*, Coast. Engng., **56**(4):419440.

[6] S. Koshizuka, H. Tamako, Y. Oka (1995), *A particle method for incompressible viscous flow with fluid fragmentation*, Comput. Fluid. Dyn. J. **4**(1):2946.

[7] A. Leroy, D. Violeau, M. Ferrand, C. Kassiotis (2014), *Unified semianalytical wall boundary conditions applied to 2-D incompressible SPH*, J. Comput. Phys. **261**:106-129.

[8] A. Leroy, D. Violeau, M. Ferrand, A. Joly (2015), *Buoyancy modelling with incompressible SPH for laminar and turbulent flows*, Int. J. Num. Meth. Fluids **78**:455474.

[9] S.J. Lind, R. Xu, P.K. Stansby, B.D. Rogers (2012), *Incompressible smoothed particle hydrodynamics for free-surface flows: A generalised diffusion-based algorithm for stability and validations for impulsive flows and propagating waves*, J. Comput. Phys. **231**:14991523.

[10] Q.W. Ma, Y. Zhou, S. Yan (2016), *A review on approaches to solving Poissons equation in projection-based meshless methods for modelling strongly nonlinear water waves*, J. Ocean Engng. Mar. Energy **2**:279299.

[11] J.J. Monaghan (2005), *Smoothed particle hydrodynamics*, Rep. Prog. Phys **68**: 17031759.

[12] J.P. Morris, P.J. Fox, Y. Zhu (1997), *Modelling low Reynolds number incompressible flows using SPH*, J. Comput. Phys., **136**:214226.

[13] A. Peer, M. Ihmsen, J. Cornelis, M. Teschner (2015), *An implicit viscosity formulation for SPH fluids*, ACM Transactions on Graphics **34**(4):114:1–114:10.

[14] S. Shao, E.Y.M. Lo (2003), *Incompressible SPH method for simulating Newtonian and non-Newtonian flows with a free surface*, Adv. Water Resources, **26**:787800.

[15] D. Violeau, A., Leroy (2014), *On the maximum time step in weakly compressible SPH*, J. Comput. Phys. **256**:388-415.

[16] D. Violeau, A. Leroy (2015), *Optimal time-step for incompressible SPH*, J. Comput. Phys. **288**:119-130.

[17] D. Violeau, B.D. Rogers (2015), *SPH for free-surface flows: past, present and future*, J. Hydr. Res. **54**(1):126.

[18] D. Violeau, S. Lind, W. Dehnen (2017), *Convergence rate of the SPH Poisson equation on a Cartesian grid*, Proc. 12th SPHERIC Int. Workshop, Ourense (Spain), June 2017.

[19] H. Wendland (1995), *Piecewise polynomial, positive definite and compactly supported radial functions of minimal degree*, Adv. Comput. Math. **4**:389-396.